Journal of Alloys and Compounds 504 (2010) 407–412

Contents lists available at ScienceDirect

Journal of Alloys and Compounds

journal homepage: www.elsevier.com/locate/jallcom

Swift heavy ion induced modifications in nano-crystalline microwave dielectric $BaTi_4O_9$ ceramics

Anjum Qureshi [a,b], Ayhan Mergen [a,*], N.L. Singh [c]

[a] Department of Metallurgical and Materials Engineering, Marmara University, Goztepe Kampusu, Istanbul 34722, Turkey
[b] Sabanci University, Faculty of Engineering and Natural Sciences,Tuzla, Istanbul 34956, Turkey
[c] Department of Physics, M.S. University of Baroda, Vadodara 390002, India

ARTICLE INFO

Article history:
Received 16 January 2010
Received in revised form 26 May 2010
Accepted 28 May 2010
Available online 8 June 2010

Keywords:
Ion irradiation
$BaTi_4O_9$
Citrate-gel processing
Dielectric properties

ABSTRACT

The pellets of $BaTi_4O_9$ were synthesized via a polymerized complex method and irradiated with 50 MeV Li^{3+} ions for two different fluences. The dielectric constant (ε_r), and dielectric loss ($\tan\delta$) as a function of frequency (1 kHz–2 MHz) and temperature (40–200 °C) were measured for unirradiated and irradiated samples. The values of ε_r for unirradiated and irradiated samples decreased with frequency at room temperature which is explained by Koops′ model. The increase in dielectric constant after the irradiation shows that the damage occurs during irradiation and produces defects due to electronic processes and/or inelastic collisions. Micro-structural properties revealed that the size of pores/holes and their number increased with irradiation fluence giving rise to volume expansion porous defects.

1. Introduction

The development of the telecommunications industry, especially in the satellite and active antennas sector requires the use of radio and microwave frequency substrates. These substrates should essentially exhibit high dielectric constant (ε_r), low dielectric loss ($\tan\delta$) and a near-zero temperature coefficient of resonant frequency (τ_f) for temperature stable circuits in the electrical devices [1]. A number of researchers have reported that TiO_2-rich compounds, such as $BaTiO_3$, $BaTi_4O_9$ and $Ba_2Ti_9O_{20}$ exhibit suitable radio and microwave dielectric properties for electrical applications [2,3].

Swift heavy ion (SHI) irradiation provides understanding of material structure damage and their modifications. The effect of energetic ion beam on the materials depends on the ion energy, fluence and ion species. The energetic heavy ions loose their energy as they pass through the material. The ions either excite or ionize the atoms by inelastic collisions or displace atoms of the target by elastic collisions. Elastic collisions are dominant in low energy regime, whereas inelastic collisions process dominates at high-energy regime where elastic collisions are insignificant. It is evident from the previous reports that electronic energy loss (S_e) due to inelastic collision can generate point/cluster of defects, if S_e is less than the threshold value of electronic energy loss (S_{eth}) [4,5]. The energetic ions can create columnar amorphization with greater value of S_e than the S_{eth}. The strain/stress developed due to the defects created by the energetic ions and amorphization enables modification in different properties of the materials [6–8]. There have been few attempts to investigate effect of irradiation on ceramic materials particularly derived of BaO–TiO_2 system [6,9,10]. Jiang et al. [6] reported irradiation-induced disorder and amorphization in $BaTiO_3$ wafers using 1 MeV Au^{2+} ions at different fluences and temperature of irradiation. It has been reported that at 170 and 300 K irradiation temperatures, the dependence of disordering was observed to be small. Recovery of disorder was also observed at low damage levels and at room temperature. The experimental investigations to the energy loss of high-energy protons (25 MeV) in $BaTiO_3$ have been reported by Kumar et al. [9]. The observed results in this study were indicative of a new mode of energy loss and can be related to the fluctuations in polarization of cluster of unit cells and the dynamics of their short-range order. The thermal phase transitions and the temperature dependence of the dose for amorphizations in $BaTiO_3$ have been investigated [10].

The dielectric properties of Ba–TiO_2 system depend upon several factors, such as chemical composition, method of preparation and grain size. Study of dielectric characteristics indicates the response of the material to an electric field. Different polarization may result into variations in the dielectric constant and dielectric loss. The purpose of this study is to understand the irradiation-induced changes

* Corresponding author at: Marmara Üniversitesi, Metalurji ve Malzeme Mühendisliği Bölümü, Göztepe kampusu, Kadıköy, Istanbul 34722, Turkey.
Tel.: +90 216 348 02 92x603; fax: +90 216 345 01 26.
E-mail addresses: ayhan.mergen@marmara.edu.tr, mergen@eng.marmara.edu.tr (A. Mergen).

0925-8388/$ – see front matter © 2010 Elsevier B.V. All rights reserved.
doi:10.1016/j.jallcom.2010.05.130

in dielectric properties and damage in micro-structures of $BaTi_4O_9$, as this material exhibit suitable dielectric properties for electrical applications. Ion beam with 50 MeV Li^{3+} was chosen because it enables higher electronic energy loss with low projected ion implantation range in the material. This eventually resulted in the modification of this material, which was investigated by dielectric and micro-structural studies. It is very useful in the study of phase transition taking place in the material before and after irradiation. The dielectric measurements as a function of frequency and temperature can provide understanding of the material modification due to the created defects by the irradiation. Therefore, the present investigation is emphasized on variations in dielectric and micro-structural properties of $BaTi_4O_9$ after irradiation. The dielectric properties were studied as a function of temperature using 50 MeV Li^{3+} ion at different fluences.

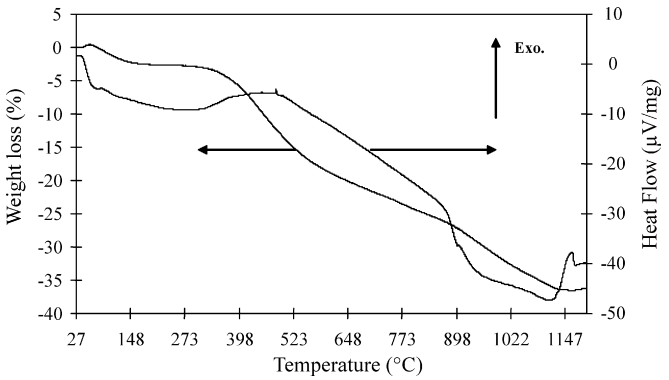

Fig. 1. TG–DTA curve of $BaTi_4O_9$ powder precursor.

2. Experimental details

$BaTi_4O_9$ powders were produced by Pechini method [11]. The starting reagents used were of high-purity and these are: barium carbonate ($BaCO_3$, 99%) and titanium isopropoxide ($Ti(OCH(CH_3)_2)_4$, 98%) supplied from Merck. Ethylene glycol ($C_2H_6O_2$) was heated to 50 °C and then added slowly with $Ti(OCH(CH_3)_2)_4$. After the milk-like solution stirred to become colorless, citric acid ($C_6H_8O_7$) was added to ethylene glycol mixture in the molar ratio of 1:10 and stirred to promote dispersion of the gel. Desired stoichiometry of $BaCO_3$ powder was then added slowly and highly dispersed by mechanical stirring. About 3–4 drops of nitric acid (HNO_3, 65%) was added to the mixture to catalyze the esterification between citric acid and ethylene glycol. The temperature was increased from 50 to 140 °C for 10 h to evaporate the solvent and promote polymerization. The pH value was 3.7 as mixtures became clear and light yellow solution. To prepare $BaTi_4O_9$ powders, the polymeric precursors were further heated at 300 °C for 1–2 h and resulted in the dark colored

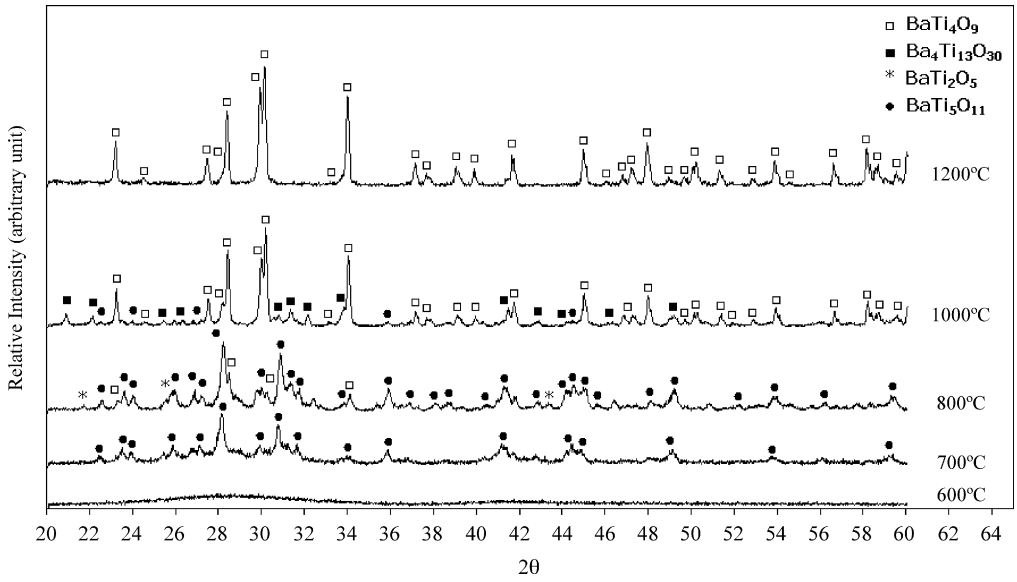

Fig. 2. XRD patterns of $BaTi_4O_9$-precursor calcined at different temperatures.

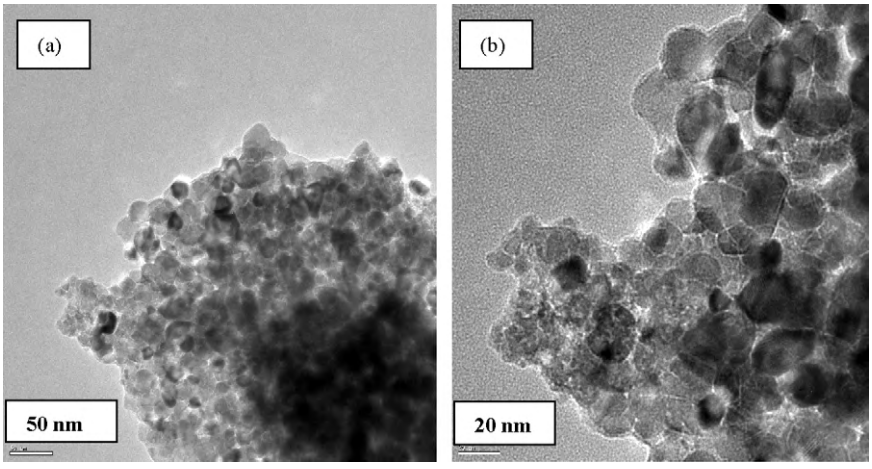

Fig. 3. TEM images of $BaTi_4O_9$ powders calcined at 1100 °C.

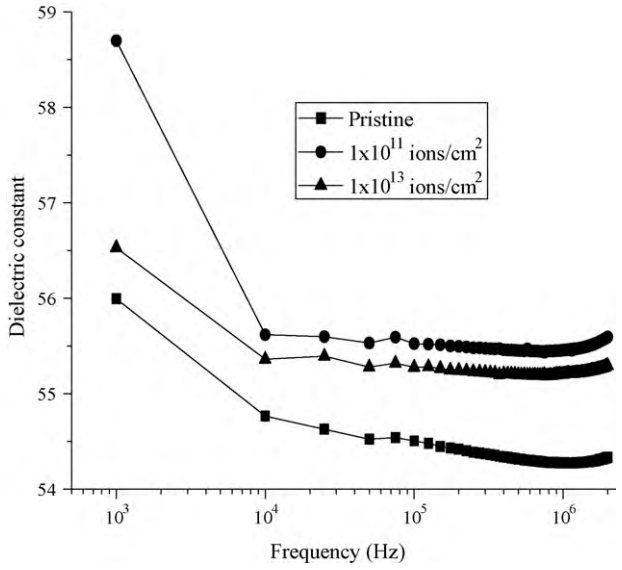

Fig. 4. Variation of dielectric constant with frequency for unirradiated and irradiated $BaTi_4O_9$ at different fluences.

amorphous citrate gels with low viscosity. The gels were calcined at 600–1200 °C for 2 h with a rate of 10 °C/min. The calcined powder was pressed into pellets of 10 mm in diameter and 1 mm in thickness. The pellets were then sintered at the temperature of 1200–1300 °C for 2 h. The densities of the ceramic pellets were measured by Archimedes method [12] and the relative density was observed to be 97.3%. The TGA thermograms of $BaTi_4O_9$ gels were recorded by Netzsch STA 449C instrument under nitrogen atmosphere at 10 °C/min heating rate. Phase identification and structural analysis were performed by X-ray diffractometer (Rigaku X-ray diffractometer) with Cu Kα radiation source (λ = 1.5406 Å) in the 2θ range of 20–60°. Surface morphology and particle size of samples were studied by transmission electron microscopy (TEM) (Tecnai G^2 F20 S-TWIN 200 kV) and scanning electron microscopy (SEM) (JEOL-5310 LV).

The specimen pellets were irradiated in vacuum with 50 MeV Li^{3+} ions at different fluences of 1×10^{11} and 1×10^{13} ions/cm^2 using 15 UD Pelletron at Inter University Accelerator Centre, New Delhi, India. The electronic, nuclear energy stopping power and projected range for 50 MeV Li^{3+} ions in the sample were calculated using SRIM (Stopping and Range of Ions in Matter-2003) code [13]. The electronic stopping power $(dE/dX)_e$, nuclear stopping power $(dE/dX)_n$ and projected range were found to be 8.669 eV/Å, 4.597×10^{-3} eV/Å, and 341.8 μm, respectively. The dielectric properties of unirradiated and irradiated samples were measured using Agilent 42841 LCR meter in the frequency range 1 kHz–2 MHz as a function of temperature. An automated measurement systems consisting of PC and a temperature chamber was used in the measurements.

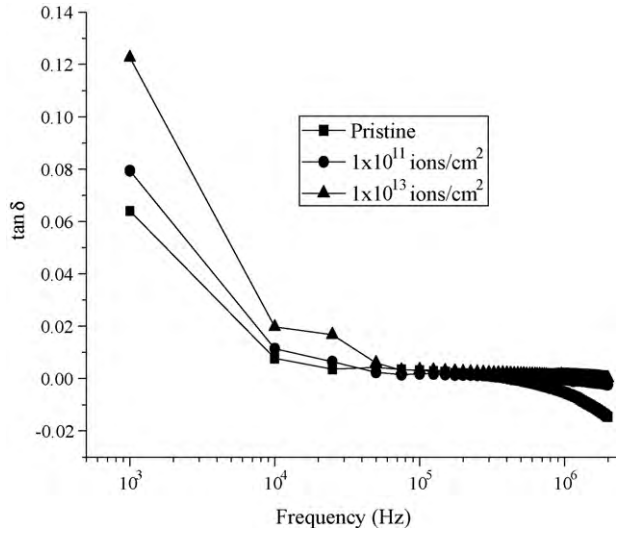

Fig. 5. Variation of dielectric loss with frequency for unirradiated and irradiated $BaTi_4O_9$ at different fluences.

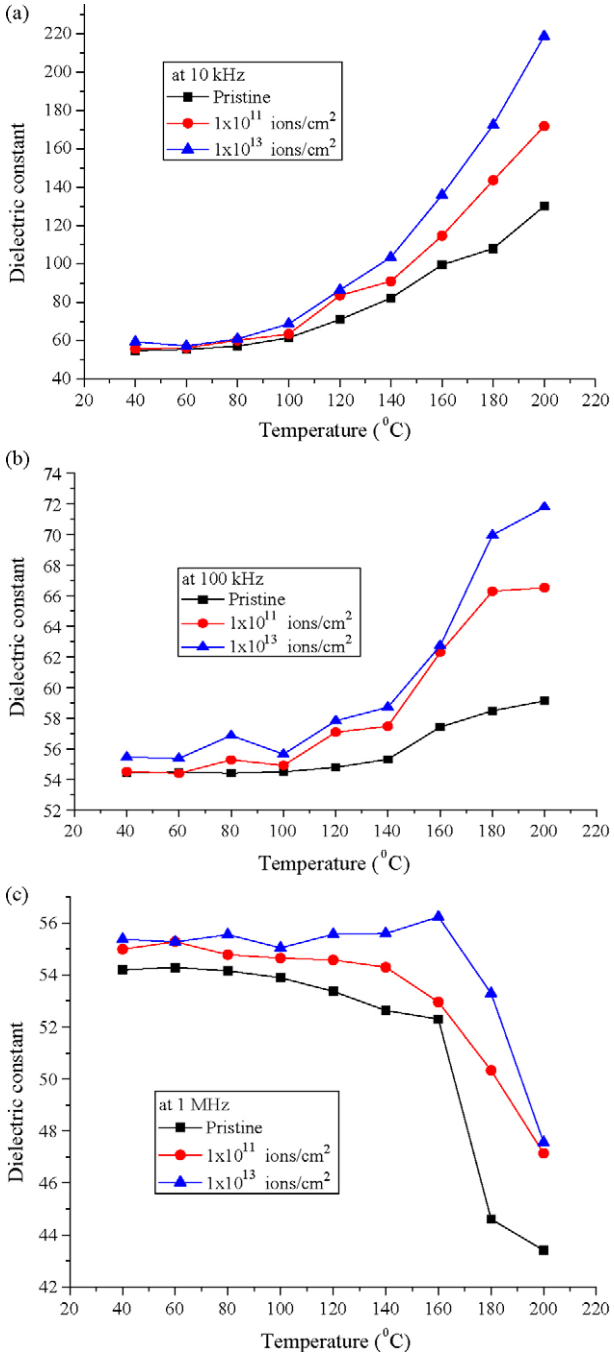

Fig. 6. Variation of dielectric constant with different temperatures (a) at 10 kHz (b) 100 kHz (c) 1 MHz frequency for unirradiated and irradiated $BaTi_4O_9$.

3. Results and discussion

3.1. Structure and morphology of $BaTi_4O_9$ nanoparticles

Fig. 1 shows the TG–DTA curves of powder precursor of $BaTi_4O_9$ heated from room temperature to 1200 °C. The TG curve (Fig. 1) shows a continuous small weight loss upto about 300 °C which is possibly due to the dehydration of precursors, evaporation of ethylene glycol and decomposition of citric acid. The major weight loss occurred after 300 °C is induced by carbonization or bond breaking of the organic moieties in the precursors [14] which gave a broad exothermic peak at around 470 °C. During this period, the polymer network break down into smaller organic moieties, and

some of these compounds which do not contain any metal ions are volatilized.

Fig. 2 shows the X-ray diffraction patterns of $BaTi_4O_9$ powders after calcinated in air at 600, 700, 800, 1000 and 1200 °C for 2 h. At 600 °C, the polymeric precursor was amorphous and no peak was observed. The first phase formed from amorphous precursors was $BaTi_5O_{11}$ (JCPDS Card No: 35-805) at 700 °C. At higher temperatures of 800 °C, the amount of $BaTi_5O_{11}$ increased and another phase of $BaTi_2O_5$ (JCPDS Card No: 34-133) also formed. $BaTi_4O_9$ phase (JCPDS Card no: 34-70) was also started to form at 800 °C. As temperature increased to 1000 °C, $BaTi_5O_{11}$ phase nearly disappeared and converted into $BaTi_4O_9$ and $Ba_4Ti_{13}O_{30}$ (JCPDS Card No: 37-75). At 1200 °C, all the peaks belong to $BaTi_4O_9$ and indicates that the single phase of $BaTi_4O_9$ formed at this temperature. Previous studies also indicate that $BaTi_5O_{11}$, $BaTi_2O_5$ and $Ba_4Ti_{13}O_{30}$ phases were intermediate phases during the formation of $BaTi_4O_9$ [14]. From the line broadening of corresponding XRD peaks, the crystallite size (D) was estimated using the Scherrer formula: $D = K\lambda/b\cos\theta$, where λ is the wavelength of the X-ray radiation, K is a constant taken as 0.9, θ is the diffraction angle and b is the full-width at half-maximum (FWHM) [15]. The particle size was determined to be 29 and 39 nm for the powders calcined at 1000 and 1200 °C, respectively.

The TEM images of $BaTi_4O_9$ powders calcined at 1200 °C exhibited the size of the particles ranging from 5 to 40 nm (Fig. 3). The particle size obtained by XRD matched well with those of TEM results. TEM images revealed spherical particle shape of $BaTi_4O_9$ and also agglomeration of powders.

3.2. Dielectric properties of $BaTi_4O_9$ before and after irradiation

The dielectric constant as a function of frequency from 1 kHz to 2 MHz is shown in Fig. 4 for unirradiated and irradiated samples. The dielectric constant for unirradiated and irradiated samples decreases with increasing frequency of the applied field, which is in agreement with Koops' model [16]. Comparing the dielectric results before and after irradiation, it shows that the damage occurs during irradiation. Generally, heavy ion irradiation produces defects due to electronic processes and/or elastic collisions. Those defects related with the electron–hole pair generation and are dose rate dependent [5]. The variation of dielectric loss with frequency is shown in Fig. 5. It was found that the values of dielectric loss increased with increasing the fluence. The loss factor is the ratio of the imaginary ε'' and the real ε' parts of the dielectric constant,

$$\varepsilon'' = \tan\delta.\varepsilon' \quad (1)$$

It is observed that after irradiation, the ε' decreases and $\tan\delta$ increases with the frequency (Figs. 4 and 5) which implies that the imaginary part ε'' of the dielectric constant increases on irradiation [17]. At lower frequencies below 10^5 Hz, the dielectric constant shows a sharp increase, this may be associated with Maxwell–Wagner mechanism (interfacial space charge) and the electrode polarization effect. The variation of dielectric constant with different temperatures at 10, 100 kHz, and 1 MHz frequencies is shown in Fig. 6. The result shows that the dielectric constant increases with temperature for both irradiated and unirradiated samples at 10 and 100 kHz frequencies (Fig. 6a and b). At low frequencies, the dipoles follow the field and we observed linear increase in dielectric constant with the temperature. Beyond 100 kHz of a frequency, the dielectric constant is constant up to a temperature of 80 °C and then started decreasing slowly with temperature (Fig. 6c). The decrease in dielectric constant with increasing frequency can be attributed to the lagging of the dipoles present in the material, which is a typical Debye behavior exhibited by most of the dielectric materials [18]. This behavior was also observed at higher frequency and at higher fluence of irradiation (Fig. 6c). Fig. 7 shows the variation of dielectric loss with frequency for unirradiated and irradiated $BaTi_4O_9$ at different temperatures. It was observed that the dielectric loss increased at the fluence of 1×10^{13} ions/cm^2 and also with temperature. It is possibly due to increase in the number of space charges that gave rise to polarization effect [17].

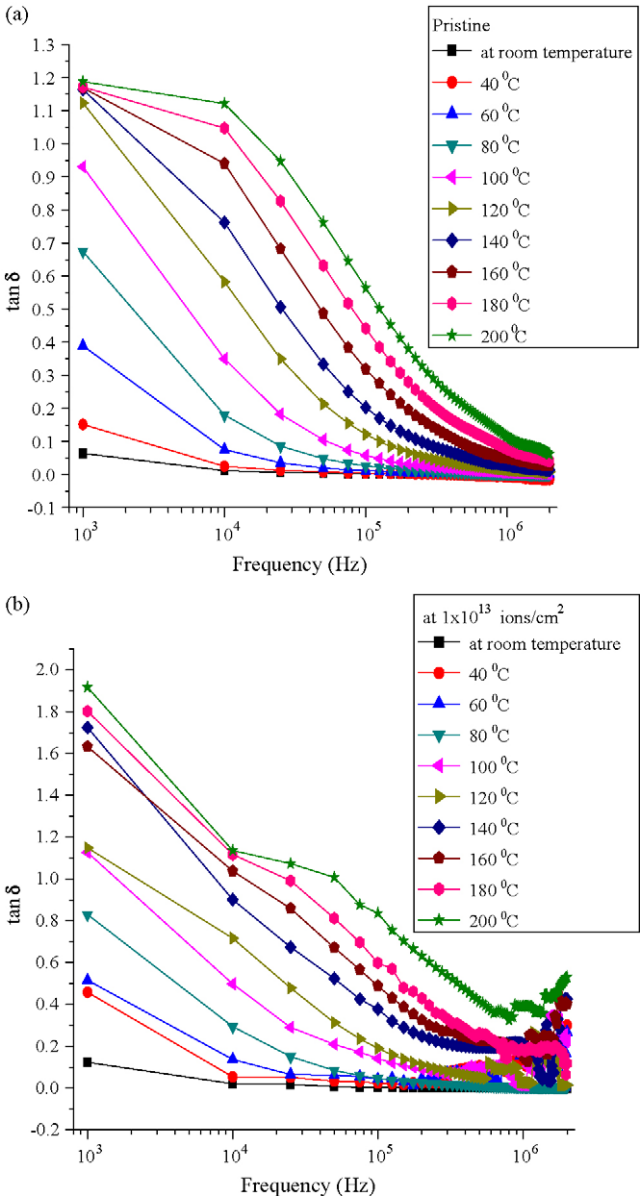

Fig. 7. Variation of dielectric loss with frequency for (a) unirradiated and (b) irradiated $BaTi_4O_9$ at different temperatures.

3.3. Micro-structural properties of $BaTi_4O_9$ before and after irradiation

SEM analysis was performed to yield information about the micro-structures of the irradiated samples. Figs. 8(a–c) and 9(a–c) shows SEM images of unirradiated and irradiated samples at the fluences of 1×10^{11} and 1×10^{13} ions/cm^2. The SEM images were captured at two different resolutions and scales. Figs. 8 and 9 show SEM images at resolution of ×500 with scale 50 μm and ×1000 with scale 10 μm, respectively. Porous structures were observed on the surfaces of the samples upon irradiation. It is clear from Figs. 8(a–c) and 9(a–c) that the pores/holes size and number increased

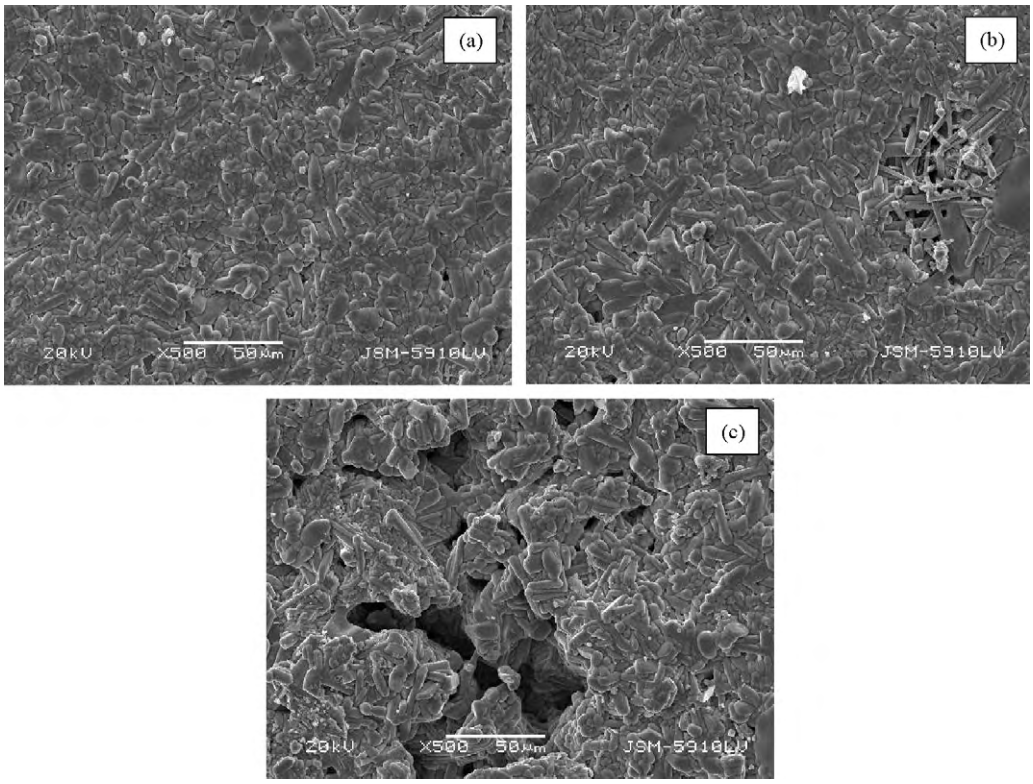

Fig. 8. The SEM images of $BaTi_4O_9$ at ×500 resolution of (a) unirradiated sample, and samples irradiated at (b) 1×10^{11} ions/cm^2 and (c) at 1×10^{13} ions/cm^2 fluences.

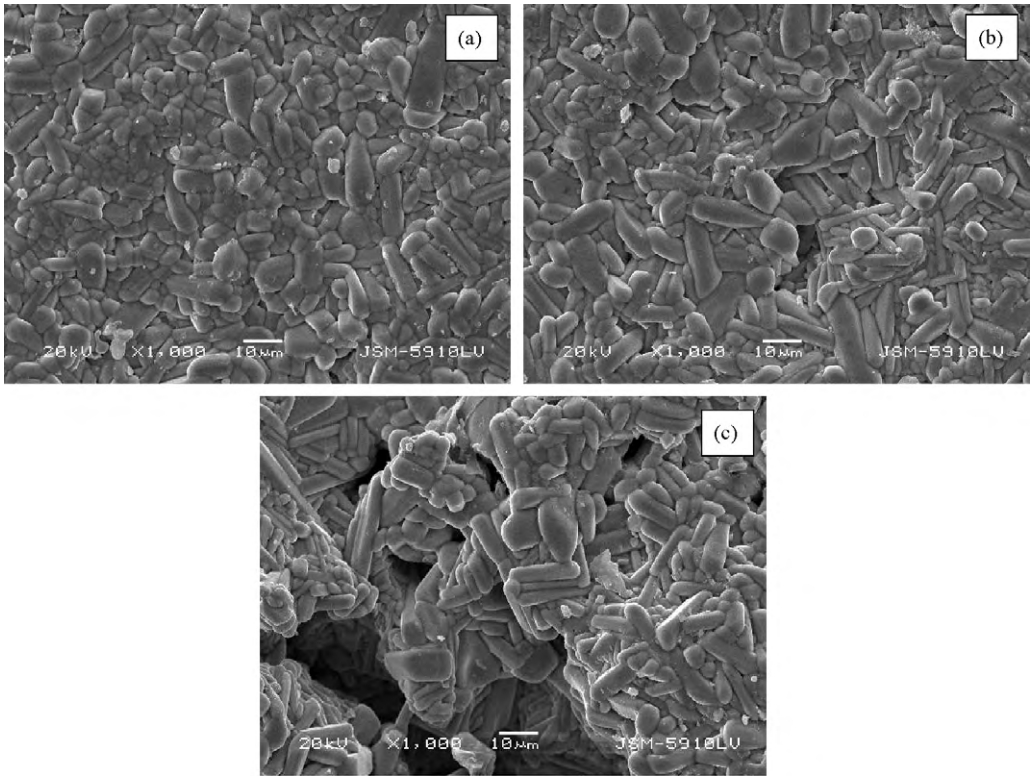

Fig. 9. The SEM images of $BaTi_4O_9$ at ×1000 resolution of (a) unirradiated sample, and samples irradiated at (b) 1×10^{11} ions/cm^2 and (c) at 1×10^{13} ions/cm^2 fluences.

with irradiation fluence that gave rise to volume expansion porous defects.

4. Conclusions

In this study, single phase $BaTi_4O_9$ ceramic was successfully synthesized by the polymeric precursor route and the dielectric and micro-structural properties of $BaTi_4O_9$ ceramic were investigated before and after ion irradiation. The dielectric response of $BaTi_4O_9$ was dependent on both temperature and fluence of irradiation. The values of dielectric constant was increased after the irradiation and decreased with the increase in the frequency of the applied field. It shows that damage occurs during irradiation and produces defects due to electronic processes and/or inelastic collisions. The value of dielectric loss was increased after the irradiation and increases with the fluence. Micro-structural properties revealed that the pores/holes size and number increased with irradiation fluence giving rise to volume expansion porous defects.

Acknowledgements

One of the authors (A.Q.) is thankful to the TUBITAK fellowship of Turkey (Project No: 107M372). We are also thankful to operating staff of Pelletron, IUAC New Delhi. Partial financial support given by IUAC New Delhi is gratefully acknowledged.

References

[1] F. Li, L.Q. Weng, G.Y. Xu, S.H. Song, J. Yu, Mater. Lett. 59 (2005) 2973–2976.
[2] C.F. Yang, C.C. Diao, H.H. Chung, H.H. Huang, H.M. Chen, J. Alloys Compd. 461 (2008) 404–409.
[3] S.B. Deshpande, P.D. Godbole, Y.B. Khollam, H.S. Potdar, J. Electroceram. 15 (2005) 103–108.
[4] B. Kaur, M. Bhat, R. Tickoo, R. Kumar, F. Licci, K. Bamzai, P. Kotrua, Ferroelectrics 323 (2005) 49–56.
[5] M. Toulemonde, C. Dufour, A. Meftah, E. Paumier, Nucl. Instr. Methods Phys. Res. B. 166 (2000) 903–912.
[6] W. Jiang, W. Weber, S. Thevuthasan, Nuc. Instr. Methods Phys. Res. B. 175 (2001) 610–614.
[7] K. Sickafus, R. Grimes, J. Valdez, A. Cleave, M. Tang, M. Ishimaru, S. Corish, C. Stanek, B. Uberuaga, Nat. Mater. 6 (2007) 217–223.
[8] G. Sattonnay, S. Moll, L. Thomé, C. Legros, M. Herbst-Ghysel, F. Garrido, J. Costantini, C. Trautmann, Nucl. Instr. Methods Phys. Res. B. 266 (2008) 3043–3047.
[9] K. Kumar, B. Kerur, S. Hanagodimath, M. Lagare, D. Avasthi, A. Mandal, Ferroelectrics 323 (2005) 65–70.
[10] G. Borstel, A. Kruminš, D. Millers, Defects and Surface-induced Effects in Advanced Perovskites, Springer, 2000.
[11] M. Weng, T. Liang, C. Huang, J. Eur. Ceram. Soc. 22 (2002) 1693–1698.
[12] M. Loverude, C. Kautz, P. Heron, Am. J. Phys. 71 (2003) 1178.
[13] J. Ziegler, Nucl. Instr. Methods Phys. Res. B 219 (2004) 1027–1036.
[14] Y. Xu, X. Yuan, P. Lu, G. Huang, Mater. Chem. Phys. 96 (2006) 427–432.
[15] C. Hammond, Basics of Crystallography and Diffraction, Oxford University Press Inc., New York, 2001.
[16] C. Koops, Phys. Rev. 83 (1951) 121–124.
[17] A. Dogra, M. Singh, V. Siva Kumar, N. Kumar, R. Kumar, Nucl. Instr. Methods Phys. Res. B 212 (2003) 184–189.
[18] S.B. Narang, D. Kaur, Ferroelectr. Lett. 36 (2009) 20–27.